Interferences from Fast Electron Emission in Molecular Photoionization

J. Fernández,[1] O. Fojón,[2] A. Palacios,[1] and F. Martín[1]

[1]*Departamento de Química C-9, Universidad Autónoma de Madrid, 28049 Madrid, Spain*

[2]*Instituto de Física Rosario (CONICET-UNR) and Escuela de Ciencias Exactas (UNR), Pellegrini 250, 2000 Rosario, Argentina*

(Received 17 July 2006; published 26 January 2007)

We present a theoretical study of fast-electron emission produced in H_2 and H_2^+ photoionization. We show that, when the electron wave length is comparable to the molecular size, the electron angular distributions arising from fixed-in-space molecules exhibit pronounced interference effects that critically depend on orientation and energy sharing between electrons and nuclei. In particular, for molecules oriented parallel to the polarization direction, the angular patterns reveal a complex nodal structure, while for molecules oriented perpendicularly, typical Young's double-slit interferences are observed. These patterns change dramatically as the molecule vibrates.

DOI: 10.1103/PhysRevLett.98.043005 PACS numbers: 33.60.Cv, 33.80.Eh

Photoionization of molecular systems is a subject that has received continuous experimental and theoretical attention for more than half a century (see, e.g., Ref. [1] for a review). In particular, the case of homonuclear diatomic molecules has been considered in great detail, since experiments are easier to analyze and the process can be accurately described by theory. Because of limitations in both electron detection efficiency and photon-source intensity, most previous studies have focused on the dominant process, i.e., the production of slow and moderately fast photoelectrons. However, the production of fast electrons offers a very interesting perspective, in particular, when the electron wave length λ_e is comparable to the size of the molecule. In this case, the wave nature of the electron should manifest through interferences and diffraction, similarly to what macroscopic waves experience when they meet a macroscopic object. The typical size of diatomic molecules is given by their internuclear distance R, and is of the order of 1 Å in most cases (e.g., 0.74 Å for H_2 and 1.06 Å for H_2^+). Therefore, interferences are expected to show up when the photon energy $h\nu$ is of the order of a hundred eV [$h\nu \sim I_p + h^2/(2m_e\lambda_e^2)$, where I_p is the vertical ionization potential]. These energies correspond to vacuum or extreme ultraviolet radiation, which is currently available in modern synchrotron radiation sources at high enough intensity.

Molecules vibrate and this can affect the way electrons are emitted. This is the case, e.g., for very slow ionized electrons, whose motion is strongly affected by the vibronic coupling between the low lying ionization continuum and the Rydberg molecular states [2,3]. This coupling is the consequence of the ionized electron having a velocity comparable to that of the nuclei; in other words, it results from the breakdown of the Born-Oppenheimer (BO) approximation. However, the faster the electron, the better is the BO approximation. Does it mean that fast electrons and vibrations do not know at all from each other? Since interferences are, in general, very sensitive to the position of the ''diffraction'' centers, it is worth investigating this question when $\lambda_e \sim R$.

An indication of the interferences associated with fast-electron emission can already be seen in the integral photoionization cross section, which approximately follows the formula [4], $\sigma_A[1 + \sin(k_eR)/(k_eR)]$, where σ_A is the atomic photoionization cross section (for an effective charge Z_{eff}) and $k_e = 2\pi/\lambda_e$ is the electron wave vector. The signature of interferences is, as usual, the oscillatory term within the brackets. However, due to the rapid decrease of σ_A with photon energy, i.e., with k_e, oscillations are usually observed in a rather indirect way, e.g., by dividing the total cross section by a ''reasonable'' independent estimate of σ_A [5,6] or by studying the ratio of two rapidly decreasing partial cross sections as in K-shell molecular photoionization [7].

Much clearer evidence of interferences can be obtained from fixed-in-space molecules. This was anticipated in 1969 by Kaplan and Markin [8] and further investigated by Walter and Briggs [9], who used a very simple model in which molecular orbitals are represented by a combination of two atomic orbitals, the continuum electron is described by a plane wave and the nuclei do not move. Experiments with fixed-in-space molecular orientations are now possible since recent imaging techniques allow one to relate the angular pattern of the ejected electrons to the orientation of the molecule at the instant of ionization [10,11]. Such imaging techniques have been inspired by previous experimental work in atoms [12], but, in contrast, in the new experiments [10,11] the momenta of all the remaining atomic and molecular ions are also determined. It has been recently shown [13] that to uncover the relevant physical effects arising from such remarkably refined experiments [10] precise quantum theoretical treatments are needed.

In this Letter we present the results of accurate theoretical calculations showing that, when $\lambda_e \sim R$, the angular distributions of electrons arising from fixed-in-space H_2^+ and H_2 molecules exhibit pronounced interference effects that critically depend on orientation and energy sharing between electrons and nuclei. More interestingly, we show that interference patterns change dramatically as the molecule vibrates, which means that the motion of fast electrons

strongly depends on the nuclei's positions. These conclusions should be of general validity for any diatomic molecule.

We restrict our study to linearly polarized light. Photoionization cross sections corresponding to leaving the residual molecular ion in a specific electronic state α, differential in (i) the photoelectron energy ϵ, (ii) the photoelectron emission direction in the molecular frame $\Omega_e = (\theta_e, \phi_e)$, and (iii) the polarization direction with respect to the molecular axis $\Omega_n = (\theta_n, \phi_n)$, $d\sigma_\alpha/d\Omega_n d\Omega_e d\epsilon$, have been evaluated in the framework of the dipole and adiabatic BO approximations using Dill's formula (15) of Ref. [14]. The transition dipole matrix element $T_{\alpha lm\mu}(\epsilon)$ is given by

$$T_{\alpha lm\mu}(\epsilon) = \int dR \langle \Psi_{g\nu}(\mathbf{r}, R) | \mathbf{e}_\mu \cdot \mathbf{D} | \Psi^+_{\alpha \upsilon_\alpha lm\epsilon}(\mathbf{r}, R) \rangle, \quad (1)$$

where $\Psi_{g\nu}$ is the ground molecular state of energy $W_{g\nu}$, $\Psi^+_{\alpha\upsilon_\alpha lm\epsilon}$ is the final molecular state of energy $W_{\upsilon_\alpha} + \epsilon$ representing a molecular ion in the υ_α vibronic state (either dissociative or nondissociative) and an ionized electron of energy ϵ and angular momentum lm, $\mathbf{r}$ represents the electronic coordinates, R is the internuclear distance, $\mathbf{e}_\mu$ is the photon polarization vector, and $\mathbf{D}$ is either $\sum_i \mathbf{r}_i$ (length gauge) or $(h\nu)^{-1}\sum_i \boldsymbol{\nabla}_i$ (velocity gauge). Energy conservation implies that $W_{g\nu} + h\nu = W_{\upsilon_\alpha} + \epsilon$. Neglecting rotational effects, the wave functions $\Psi_{g\nu}$ and $\Psi^+_{\alpha\upsilon_\alpha lm\epsilon}$ are evaluated in the adiabatic BO approximation

$$\Psi_{n\upsilon_n}(\mathbf{r}, R) = R^{-1}\chi_{\upsilon_n}(R)\psi_n(\mathbf{r}, R), \quad (2)$$

where ψ_n and χ_{υ_n} are the usual electronic and nuclear BO wave functions. For each value of R, the electronic continuum states must satisfy the usual outgoing boundary conditions of electron-molecule scattering.

Dill's formula has been used to obtain the electron angular distribution from fixed-in-space H_2^+ and H_2 molecules at a particular energy sharing between the ejected electron and the remaining ions (3D polar plots in Figs. 1 and 2). Integrating that formula over the azimuthal angle ϕ_e leads to the differential cross sections $d\sigma_\alpha/d\Omega_n \times \sin\theta_e d\theta_e d\epsilon$ given in panel (c) of Figs. 1 and 2, and further integration over the polar angle θ_e gives the cross section for fixed-in-space molecules differential in the energy of the ejected electron $d\sigma_\alpha/d\Omega_n d\epsilon$ (or, equivalently, differential in the energy of the residual ions W_{υ_α}) irrespective of the emission direction [panel (b) of Figs. 1 and 2]. Finally, integration over electron energy leads to the total photoionization cross section for fixed-in-space molecules, $d\sigma_\alpha/d\Omega_n$ [panel (a) of Figs. 1 and 2].

The computational methods used in this Letter to obtain the electronic and vibrational wave functions make use of B-spline functions and are similar to those successfully applied to study a variety of ionization problems in H_2, such as resonant dissociative photoionization [15,16] and ion impact ionization [17]. They have also led to the first

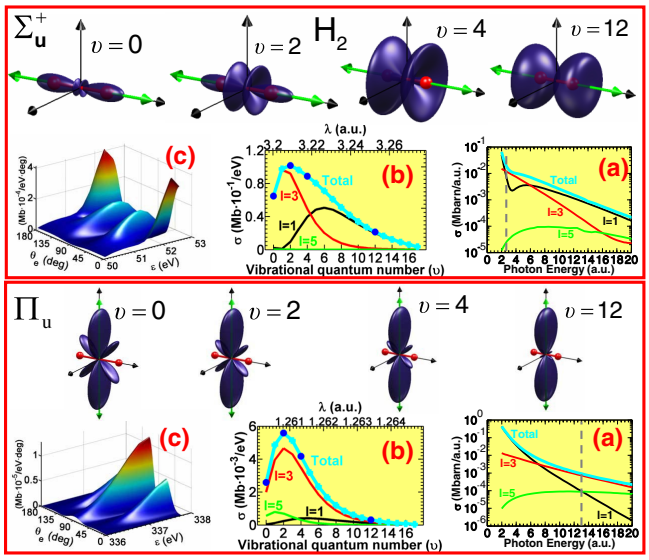

FIG. 1 (color online). Nondissociative photoionization of the H_2 molecule using linearly polarized light parallel (upper box, Σ_u^+ symmetry) and perpendicular (lower box, Π_u symmetry) to the molecular axis. (a) Integrated photoionization cross section $d\sigma_\alpha/d\Omega_n$ as a function of photon energy; contributions from different partial waves are indicated with different colors; the vertical dashed line indicates a photon energy of 2.5 a.u. (~68 eV) for the parallel arrangement and 13 a.u. (~350 eV) for the perpendicular arrangement. For the chosen photon energies, panel (b) shows the vibrational distribution of the remaining $H_2^+(\upsilon)$ ions and the contribution of the different partial waves, and panel (c) shows the differential photoionization cross sections $d\sigma_\alpha/d\Omega_n \sin\theta_e d\theta_e d\epsilon$. The 3D plots show the fully differential electron angular distribution, $d\sigma_\alpha/d\Omega_n d\Omega_e d\epsilon$, for the chosen photon energy and four selected energy sharings [indicated by blue circles in panel (b)]. For a better visualization, all 3D plots have been normalized to 1 at the maximum of the electron angular distribution.

numerical solution of the complete photoinduced breakup of H_2 [13]. We refer the reader to those works and, for more details, to the reviews of Refs. [16,18]. It must be noted, however, that due to the strong oscillatory behavior of the fast-electron continuum wave functions and the high sensitivity of the fully differential cross sections to small deficiencies in the wave functions, convergence has been achieved only by using a much larger number of partial waves (up to $l = 20$) and B splines (~400 per l) within a box of 60 a.u.

Figures 1 and 2 present the results for H_2 and H_2^+, respectively. Panel (a) shows the integrated (in electron energy and solid angle) cross section as a function of photon energy for polarized light parallel (Σ_u^+ symmetry) and perpendicular (Π_u symmetry) to the molecular axis. For H_2 (Fig. 1), only the dominant nondissociative contribution [$H_2^+(1s\sigma_g) + e^-$] is given. Let us first consider the results obtained in the parallel Σ_u^+ arrangement (upper box in Figs. 1 and 2). For this arrangement, the different partial waves (denoted by l) exhibit pronounced minima at very specific photon energies. These minima lead to shallow

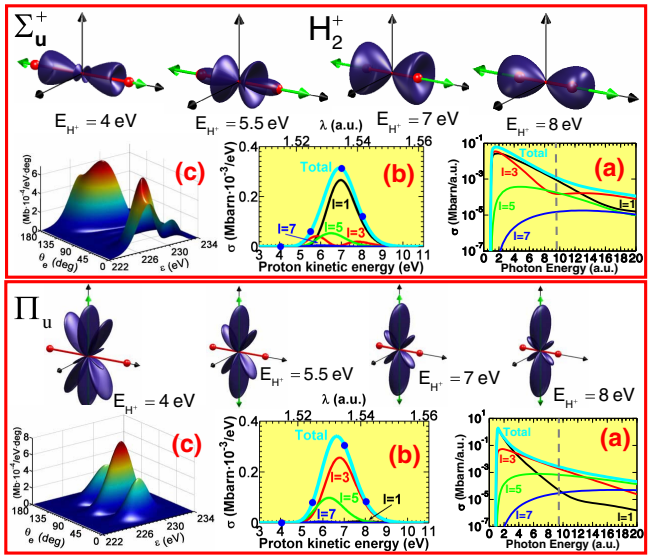

FIG. 2 (color online). Photoionization of the H_2^+ molecule using linearly polarized light parallel (upper box, Σ_u^+ symmetry) and perpendicular (lower box, Π_u symmetry) to the molecular axis. Conventions as in Fig. 1, except that the chosen photon energy is now 9.5 a.u. (~250 eV).

dips in the total photoionization cross section. Similar minima have also been found in calculations in which the position of the nuclei is frozen [19–21]. Inclusion of the nuclear motion barely affects the positions of these minima, but it does change their shape and, as we will see below, has profound implications in the analysis of differential cross sections. From the results shown in Figs. 1(a) and 2(a) for the Σ_u^+ symmetry, we find that, for each partial wave, the first minimum appears when the electron wave vector satisfies $k_e R \sim l\pi$. According to this simple formula, the $l = 1$ minimum should appear at $h\nu \sim 3.1$ a.u. for H_2 and ~2.3 a.u. for H_2^+, and the $l = 3$ minimum at ~23 a.u. and ~12 a.u., respectively. These values are in reasonable agreement with the actual ones in the figures. For H_2^+, the $l = 1$ minimum appears at such low photon energies that the $l = 3$ partial wave unexpectedly dominates in that region (in contrast with the $l = 1$ dominance observed in most diatomic molecules at low photon energies, e.g., in H_2). The $k_e R = l\pi$ formula describes momentum quantization of an electron moving inside a one-dimensional box of length R. This suggests that the observed minima can be related to electron confinement at a given internuclear distance. Indeed, we have checked that, for the k_e values satisfying this condition, the electron continuum wave functions approximately reproduce the nodal structure of the bound $nl\sigma_u$ molecular orbitals in the internuclear region (i.e., $2p\sigma_u$, $4f\sigma_u$, ... for $l = 1, 3, \ldots$, respectively). For the perpendicular Π_u arrangement [panel (a) in the lower box of Figs. 1 and 2], a similar effect is not observed.

At a given photon energy, the electron wave length λ_e depends on the energy sharing between the ionized electron and the residual ion: $W_{g\nu} + h\nu = W_{v_\alpha} + h^2/(2m_e\lambda_e^2)$. Panel (b) in Figs. 1 and 2 shows the differential (in λ_e or equivalently in the energy of H_2^+ —for H_2— and H^+ —for H_2^+ —) cross sections and the contribution of the different partial waves for the photon energies indicated by vertical dashed lines in panel (a). In the Σ_u^+ case, the chosen photon energy is close to one of the relevant minima in the partial cross sections (i.e., where confinement is expected to occur). It can be seen that the relative contributions of the different partial waves depend on the energy of the ejected electron (i.e., on the energy of the H_2^+ and H^+ nuclear fragments). This implies very different angular distributions for different energy sharings [see panel (c) and the three dimensional polar plots shown in Figs. 1 and 2]. In the case of H_2 photoionization with polarized light parallel to the molecular axis (top of Fig. 1), the angular distribution of the fastest electrons (i.e., of those electrons associated with a residual H_2^+ ion in a low vibrational state) exhibits an almost perfect f shape ($l = 3$). As we consider slower and slower electrons (i.e., H_2^+ in higher vibrational states), the $l = 1$ and $l = 3$ waves interfere leading to a complicated angular pattern, until $l = 1$ dominates and an almost pure p wave is found. These variations in the electron angular distribution are also responsible for the non—Franck-Condon vibrational distribution of the residual H_2^+ ion (a Franck-Condon distribution decreases much faster with v). Similar strong variations have been obtained in this parallel arrangement for H_2 dissociative ionization (not shown) and for H_2^+ (top of Fig. 2).

When the polarization is perpendicular to the molecular axis (Π_u symmetry shown in the lower box of Figs. 1 and 2), the angular distribution is quite different: a dominant lobe appears along the polarization direction accompanied by smaller lobes on each side. The calculated angular distributions remind us of the interference patterns observed in Young's double-slit experiment. It can be seen that the larger the energy of the ejected electron, the larger the relative intensity of the smaller lobes. For sufficiently large electron energies, additional lobes can be observed.

Several simple images can be invoked to understand the observed features. All of them are based on a one-to-one mapping between the energy of the residual ion and R. This is a reasonable assumption in the case of H_2^+ photoionization, since electron emission is followed by the Coulomb explosion of the remaining protons. Assuming that the protons behave classically, it is then possible to relate the observed proton kinetic energy to the R value at which Coulomb explosion takes place, $2E_{H^+} \sim 1/R$ [10]. This is usually called the reflection approximation. Thus the analysis of the electron angular distribution for different kinetic energies of the ejected electron (or different energies of the residual protons) at a fixed photon energy allows one to visualize the variation of the interference patterns as the molecule vibrates. Such temporal pictures can be obtained by measuring in coincidence the momentum of all ejected particles [10,11]. In the context of this approxima-

tion, the positions of all the lobes observed in the perpendicular orientation follow, to a very good approximation, Young's formula $R\sin\theta_e = n\lambda_e$, $n = 1, 2, \ldots$. Similarly, for the parallel orientation, electron confinement is only possible when the vibrating H_2^+ is ionized at a value of the internuclear distance compatible with the condition $k_e R = l\pi$. Indeed, Fig. 2 shows that, for $h\nu = 9.5$ a.u., electron confinement occurs for a proton kinetic energy $E_{H^+} \sim 6$ eV ($k_e \sim 4.1$ a.u., hence $\lambda_e \sim 1.5$ a.u.). According to the reflection approximation, $R \sim 2.3$ a.u., which satisfies $k_e R \sim 3\pi$, in agreement with the fact that the $l = 3$ partial wave suffers confinement. When ionization occurs at longer or shorter internuclear distances, there is no confinement, which explains the abrupt variations in the electron angular distribution in a narrow interval of proton kinetic energies around 6 eV. For either orientation, the angular distributions approximately follow the formula [9] $(\mathbf{e}_\mu \cdot \mathbf{k}_e)^2 \cos^2(\mathbf{k}_e \cdot \mathbf{R}/2)$. If $\mathbf{e}_\mu$ and $\mathbf{k}_e$ are parallel to the molecular axis, this formula leads to zero when $k_e R = \pi$, 3π, ..., i.e., no electron emission along the molecular axis in agreement with the image of confinement. A similar formula describes in classical optics the interference produced at long distances by two radiating dipole antennas separated a distance R. Nevertheless, one must be careful in using this analogy for quantitative analysis since it is not valid when $r \sim R$.

For H_2, the predictive value of the above models is more limited since the remaining molecular ion is mainly left in a bound vibrational state and one cannot rely on the reflection approximation. According to previous work [22,23], one can expect that different vibrational states of the residual ion sample a narrow enough subset of R values, so that the above picture remains approximately valid. We have checked that this is the case if R is chosen around the mean value of the inner and outer classical turning points associated with the final vibrational state of the residual H_2^+ ion. However, electron correlation, which plays an important role in the bond region, cannot be accounted for by any of the above models.

In summary, the analysis of the electron angular distribution arising from fixed-in-space molecules irradiated with high frequency polarized light can provide unprecedented insight of interference effects in one-photon molecular ionization. In the case of linearly polarized light perpendicular to the molecular axis, the observed pattern is very similar to that of an oscillating double slit. In the case of linearly polarized light parallel to the molecular axis, the ionized electron can be transiently confined between the nuclei and, consequently, can escape without following the polarization direction. Finally, the analysis of the electron angular distribution for different electron-ion energy sharings provides a picture of the time evolution of such interferences as the molecule vibrates.

Work supported by the DGI Project No. BFM2003-00194, the AECI Project No. A/3067/05, the European COST action D26/0002/02, and the BSCH-UAM agency. We thank the CCC-UAM for computer time.

[1] Y. Hatano, Phys. Rep. **313**, 109 (1999).
[2] R. S. Berry and S. E. Nielsen, Phys. Rev. A **1**, 383 (1970).
[3] R. S. Berry and S. E. Nielsen, Phys. Rev. A **1**, 395 (1970).
[4] H. D. Cohen and U. Fano, Phys. Rev. **150**, 30 (1966).
[5] N. Stolterfoht *et al.*, Phys. Rev. Lett. **87**, 023201 (2001).
[6] D. Misra *et al.*, Phys. Rev. Lett. **92**, 153201 (2004).
[7] X. J. Liu *et al.*, J. Phys. B **39**, 4801 (2006).
[8] I. G. Kaplan and A. P. Markin, Sov. Phys. Dokl. **14**, 36 (1969).
[9] M. Walter and J. Briggs, J. Phys. B **32**, 2487 (1999).
[10] T. Weber *et al.*, Nature (London) **431**, 437 (2004).
[11] D. Rolles *et al.*, Nature (London) **437**, 711 (2005).
[12] B. El-Marji, J. P. Doering, J. H. Moore, and M. A. Coplan, Phys. Rev. Lett. **83**, 1574 (1999).
[13] W. Vanroose, F. Martín, T. N. Rescigno, and C. W. McCurdy, Science **310**, 1787 (2005).
[14] D. Dill, J. Chem. Phys. **65**, 1130 (1976).
[15] I. Sánchez and F. Martín, Phys. Rev. Lett. **82**, 3775 (1999).
[16] H. Bachau, E. Cormier, P. Decleva, J. E. Hansen, and F. Martín, Rep. Prog. Phys. **64**, 1815 (2001).
[17] G. Laurent, J. Fernández, S. Legendre, M. Tarisien, L. Adoui, A. Cassimi, X. Fléchard, F. Frémont, B. Gervais, and E. Giglio *et al.*, Phys. Rev. Lett. **96**, 173201 (2006).
[18] F. Martín, J. Phys. B **32**, R197 (1999).
[19] P. D. M. Brosolo and A. Lisini, Chem. Phys. **181**, 85 (1994).
[20] S. K. Semenov and N. A. Cherepkov, J. Phys. B **36**, 1409 (2003).
[21] O. A. Fojón, J. Fernández, A. Palacios, R. D. Rivarola, and F. Martín, J. Phys. B **37**, 3035 (2004).
[22] J. L. Dehmer, D. Dill, and S. Wallace, Phys. Rev. Lett. **43**, 1005 (1979).
[23] T. Jahnke *et al.*, Phys. Rev. Lett. **93**, 083002 (2004).